Available online at www.sciencedirect.com

SCIENCE DIRECT

Surface & Coatings Technology 194 (2005) 96–102

SURFACE & COATINGS TECHNOLOGY

www.elsevier.com/locate/surfcoat

Microstructure modifications and phase transformation in plasma-sprayed WC–Co coatings following post-spray spark plasma sintering

H. Li[a], K.A. Khor[a,*], L.G. Yu[a], P. Cheang[b]

[a] *Fuel Cell Strategic Res. Programme, School of Mechanical and Production Engineering, Nanyang Technological University, 50 Nanyang Avenue, Singapore 639798, Singapore*

[b] *School of Materials Engineering, Nanyang Technological University, 50 Nanyang Avenue, Singapore 639798, Singapore*

Received 28 January 2004; accepted in revised form 30 April 2004
Available online 15 July 2004

Abstract

Thermal sprayed tungsten carbide (WC)–cobalt (Co) coatings have been extensively employed as abrasion/wear protective layers. However, carbon loss (decarburization) of WC–Co powders during thermal spraying reduces the efficiency of the coatings against abrasive wear. Post-spray treatment with spark plasma sintering (SPS) technique was conducted on plasma-sprayed WC–Co coatings in the present study with the aim to compensate the lost carbon in the coatings. X-ray diffraction (XRD), scanning electron microscope (SEM), and transmission electron microscope (TEM) were utilized to characterize the microstructure and phase changes in the coatings brought about through the SPS treatment. Results showed that the rapid SPS technique is successful in supplying superfluous carbon for the restoration of WC in the coating through phase transformation from W_2C or reaction with W. Predominant presence of WC was revealed in the coatings treated with SPS at 800 °C and up to 6 min. Furthermore, changes in microstructure, e.g., grain size growth, redistribution of various indigenous phases, were revealed within the coatings after the SPS treatment. It was found that the SPS-induced WC reconstruction can apparently be achieved within the coating surface with limited thickness (<10 μm). Transmission electron microscopy (TEM) results also showed the evidence of supplementary reaction between Co and WC/W_2C to form Co_3W_3C during the SPS processing. Microhardness values obtained on the surface of SPS-treated coating showed ~40% enhancement over as-sprayed surface.

Keywords: WC–Co; Plasma spray; Spark plasma sintering; Decarburization; Phase transformation; Microstructure

1. Introduction

Among the non-oxide engineering materials, carbides play an important role in resisting wear and corrosion at either ambient or high temperatures. Tungsten carbide (WC) has been well-known for its exceptional hardness and wear/erosion resistance. Matrices of ductile metals, such as cobalt (Co), greatly improve its toughness so that brittle fracture can be effectively avoided during operation. WC–Co coatings were extensively used to enhance the wear resistance of various engineering components, e.g., cutting tools. There are generally two dominant thermal spray methods for WC–Co coating deposition: plasma spray and high-velocity oxy-fuel (HVOF) processes. The study on thermal sprayed WC–Co coatings has been conducted [1–4] towards a successful application in various industries. Generally, plasma spray was widely utilized owing mainly to economic considerations. Due to the high flame temperatures (typically >5000 °C), a satisfactory melt state of sprayed powders can be assured, which is beneficial for the formation of a dense coating structure. However, for all WC–Co systems, due to phase decomposition or oxidation, the loss of carbon (decarburization) during plasma spray coating deposition is very common [5–7]. Some researchers pointed out that the decarburization mainly occurred as the oxidization of carbon, which came from extensive dissolution of WC in Co [6]. Whilst Li et al. [8] found that the rebounding of bulky carbide particles was also responsible for the carbon loss. These phenomena directly resulted in the significant loss of carbide, which is undeniably detrimental since the decarburization-resulted phases, e.g., W_2C, W, are weaker

* Corresponding author. Tel.: +65-6790-5526; fax: +65-6791-1859.
E-mail address: mkakhor@ntu.edu.sg (K.A. Khor).

0257-8972/$ - see front matter © 2004 Elsevier B.V. All rights reserved.
doi:10.1016/j.surfcoat.2004.04.075

Table 1
Parameters for the plasma spraying and SPS post-spray treatment

Plasma spraying	SPS processing
Net energy: 14 kW	SPS temperature: 800 °C
Flow of argon: 82 scfh	Duration: 6 min
Flow of helium: 44 scfh	Heating rate: 100 °C/min
Flow of carrier gas (argon): 14 scfh	Punch pressure: 10 MPa
Powder feeding rate: 20 g/min	
Distance: 12 cm	

than the original WC in resisting wear. The decarburization, accompanied by the formation of W_2C or W during thermal spraying of WC–Co, also result in decreased mechanical properties, e.g., the loss of inter-splat adhesion, which is responsible for the degradation of mechanical properties [9]. For the decarburization of WC during the spraying process, a model has been proposed that accounts for the microstructure features observed in the coatings [10]. Stewart et al. [10] reported that the decarburization involves melting of cobalt during the spray process, dissolution of WC into the molten cobalt, loss of carbon from the periphery of the particles through oxidation, which thus promotes further WC dissolution locally, and quenching of the particles which results in the formation of an amorphous binder phase, and precipitation of W_2C or W depending on the degree of decarburization.

However, unfortunately, the decarburization is unavoidable due to the high temperature attained by the particles during the WC–Co plasma spray coating deposition. To date, there is no report on reversing W_2C or W to WC after the coating deposition. Available attempts were focused on altering the process settings, e.g., HVOF [1], cold spray [3],

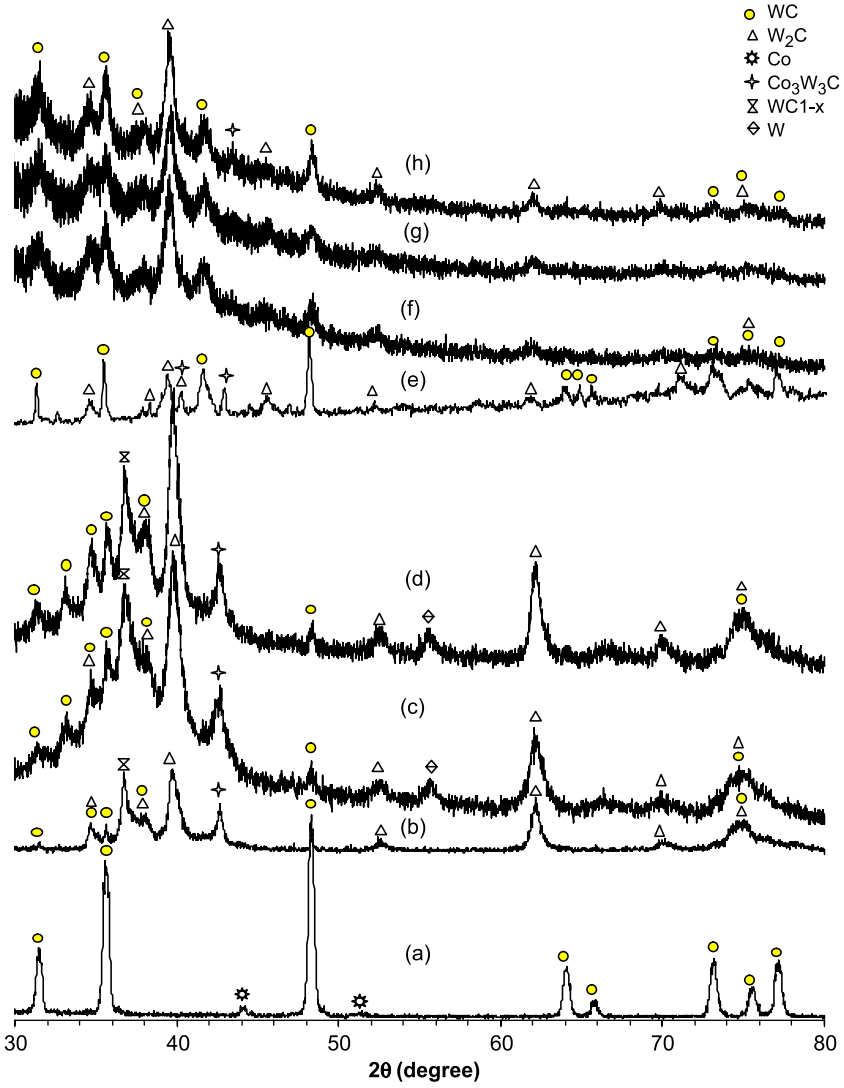

Fig. 1. XRD patterns of as-plasma-sprayed and SPS post-spray treated WC–12Co coatings, (a) starting WC–12Co powders (traditional XRD), (b) as-plasma-sprayed WC–12Co coating (traditional XRD), (c) thin film XRD curve obtained from surface of the as-sprayed coating, (d) thin film XRD curve detected from polished surface (20 μm removed) of the as-sprayed coating, (e) curve detected from surface of the SPS-treated coating (traditional XRD), (f) thin film XRD curve detected from surface of the SPS-treated coating (~ 10 μm removed), (g) thin film XRD curve obtained from polished surface of the SPS-treated coating (~ 14 μm removed) and (h) thin film XRD curve obtained from further polished surface of the SPS-treated coating (~ 34 μm removed).

and optimizing spray parameters [9]. A previous report revealed that spark plasma sintering (SPS), a rapid sintering technique, was capable of restoring WC in the plasma-sprayed WC–Co coatings [11]. The present paper presents further analysis on the microstructural changes of the coatings brought about by the SPS post-spray treatment. A possible WC restoration mechanism is also offered.

2. Experimental details

WC–12Co powders (Praxair 1342VM/WC-72701, −45 μm+15 μm) were sprayed using a fully computerized 100 kW model 4500 plasma spray system (Praxair Thermal Spray, USA). Plasma spray parameters for the WC–Co coating deposition are tabulated in Table 1, in which the SPS parameters are also demonstrated. The SPS parameters were selected according to previous studies, which found the set of parameters that is most suitable for the reversion of W_2C to WC. The SPS post-spray treatment used direct contact of the graphite punch with the coating samples. As-sprayed surface and cross-sectional morphology of the coatings was observed by means of a scanning electron microscope (SEM, JEOL JSM-5600LV, Japan) and transmission electron microscope (TEM, JEOL, JEM-2010, Japan) at 200 kV. Phase composition of the starting powders and the coatings was analyzed by X-ray diffraction (XRD) method (MPD 1880, Philips, The Netherlands). The operating conditions were 40 kV and 30 mA by using Cu Kα radiation. The goniometer was set at a scan rate of 0.015°/s over a 2θ range of 20–80°. Thin film XRD characterization was also conducted using Cu Kα radiation at 50 kV/20 mA (*Rigaku*, *Japan*).

3. Results and discussion

Fig. 1 shows the XRD slots of SPS-treated coating samples with a comparison with the original powders and as-sprayed coatings. Also, the XRD curves obtained through both conventional XRD and thin film XRD are compared in the figure. The typical thin film XRD (TF-XRD) pattern for the top layer of the SPS-treated coating is shown in Fig. 2. It is obvious that, compared to the as-sprayed coatings, the SPS-treated samples show a significant increase in the relative content of WC (curve 'e' compared to curve 'b' in Fig. 1). It did prove that the decarburization (defined here as the carbon loss from WC) during the plasma spraying WC–12Co is remarkable (curve 'b' vs. curve 'a' in Fig. 1) with the appearance of W_2C and other phases besides WC. Thin film XRD analysis (Fig. 1c,d) suggests that the as-plasma-sprayed coating has evenly distributed phases, that is, the phases presenting at coating surface are similar to those presenting within the coating. It is noted that the W peak is, unfortunately, observable only on the thin film XRD curves (Fig. 1c,d). The reason why W is only detectable through the thin film XRD is still not clear. Nevertheless, the decarburization/restoration of WC is obvious through the comparison among the XRD curves. The top layer of the SPS-treated WC–Co coating showed virtually complete WC restoration (Fig. 2). The graphite detected at the top surface of the SPS WC–Co sample (Fig. 2) is quite likely from the graphite punch. It shows that for the WC that formed through SPS treatment, a preferred orientation of WC was revealed ((001) face shown in Fig. 2). However, it must be noted that the WC restoration effect is detectable only for a thin layer (Fig. 1e compared to Fig. 1f). It nevertheless proved that, for the WC–Co coating with a thickness <10 μm, the SPS treatment brought about significant restoration of WC (Fig. 1e).

The changes in microstructure of the WC–Co coating before and after the SPS treatment were revealed through TEM observation. The as-sprayed coating shows a nanostructure, which contains nanosized grains (<50 nm) of both WC and W_2C (Fig. 3). A predominant presence of W_2C was revealed in the as-sprayed coatings. In the SPS-treated coating, however, a strong presence of WC was

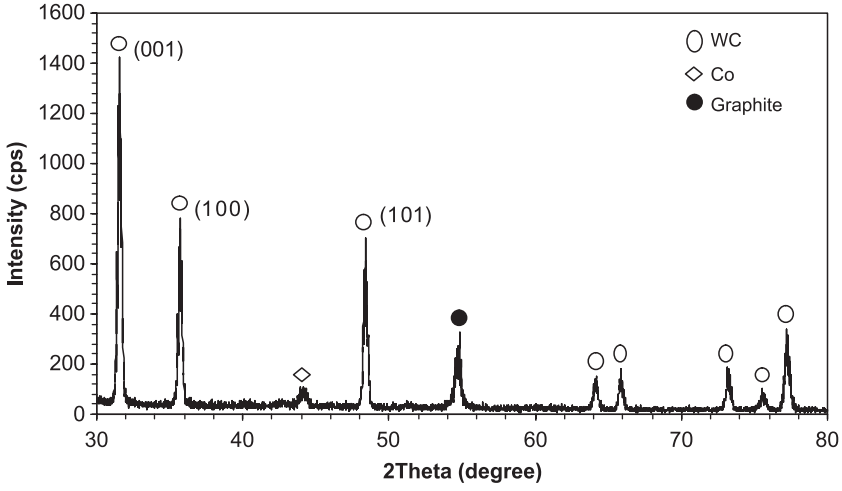

Fig. 2. Thin film XRD pattern of the top layer of the SPS-treated WC–Co coating showing a full restoration of WC.

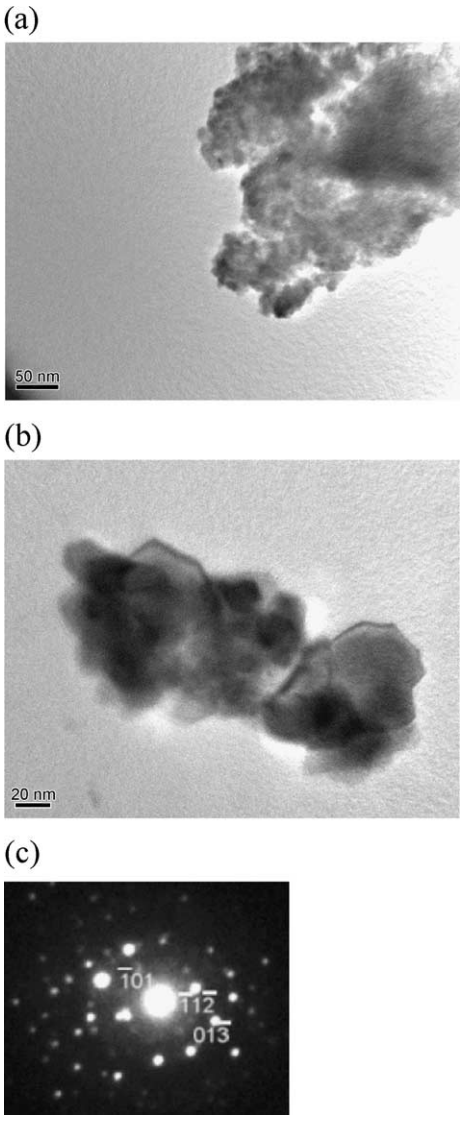

Fig. 3. Typical TEM microstructure of the as-sprayed WC–Co coating showing (a, b) nanosized WC/W_2C grains; (c) shows a SAD pattern taken from the biggest grain in (b), suggesting the W_2C phase with hexagonal structure from the [131] zone.

revealed (Fig. 4). A Co layer surrounded the WC/W_2C grains (Fig. 4). Also, it was found that correspondingly W_2C grains are surrounded with WC grains (Fig. 5), which suggests importance of carbon diffusion for the formation of WC from W_2C. The mechanism might be that carbon diffusion through grain boundaries during the SPS processing results in the transformation of W_2C to WC through $W_2C + C \rightarrow 2WC$. The presence of W_2C grain after the SPS processing (Fig. 5) suggests insufficient carbon diffusion, and hence, incomplete WC restoration. Therefore, the processing time and pressure applied on the coating sample would influence the extent of the WC restoration. It shows that the W_2C grains formed during the coating deposition are of smaller size than the original WC grains. Combining with the XRD results (Figs. 1 and 2), it is believed that the limited diffusion of carbon during the SPS processing is responsible for the lower W_2C to WC reversion rate. Furthermore, through the TEM characterization, it is interesting to note that a layer of Co_3W_3C (~ 80 nm in thickness) within the SPS-treated coating samples was revealed (Figs. 6 and 7). Also, it is found that the Co_3W_3C layer is located at the place between Co layer and WC/W_2C area (Fig. 6). Compared to the as-sprayed coating, the SPS-treated WC–Co indicates an intensified reaction between Co and WC.

The formation of W_2C, W and the η phase (e.g., Co_3W_3C) can be well explained by the mutual behaviors among the components during the high-temperature plasma spraying. Fig. 8 shows the phase changes in WC–Co at the temperature 1425 °C [12]. Cobalt may diffuse into the

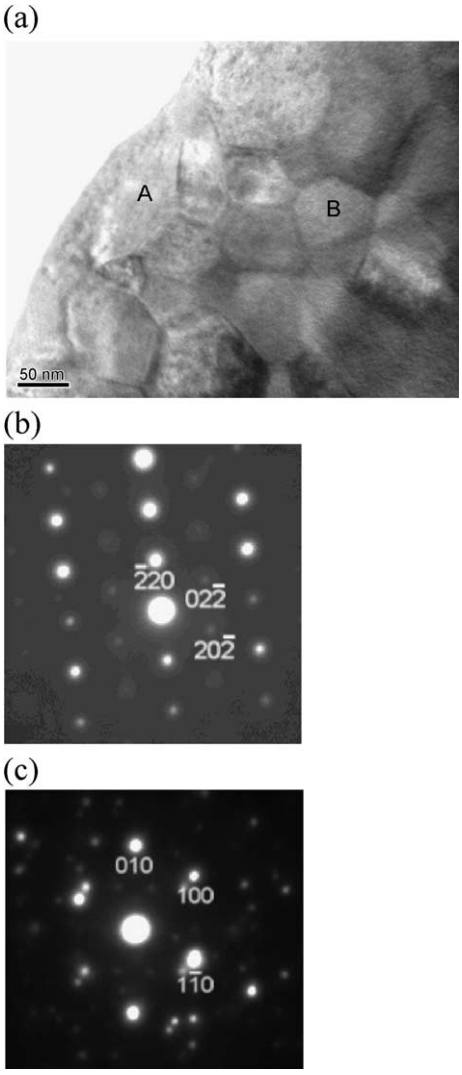

Fig. 4. Typical TEM microstructure of the SPS-treated WC–Co coating (a) showing that WC grains are surrounded by Co layer; (b) shows a SAD pattern taken from the area A in (a), suggesting Co with cubic structure from [111] zone; and (c) shows a SAD pattern taken from the area B in (a), suggesting WC with hexagonal structure from the [001] zone.

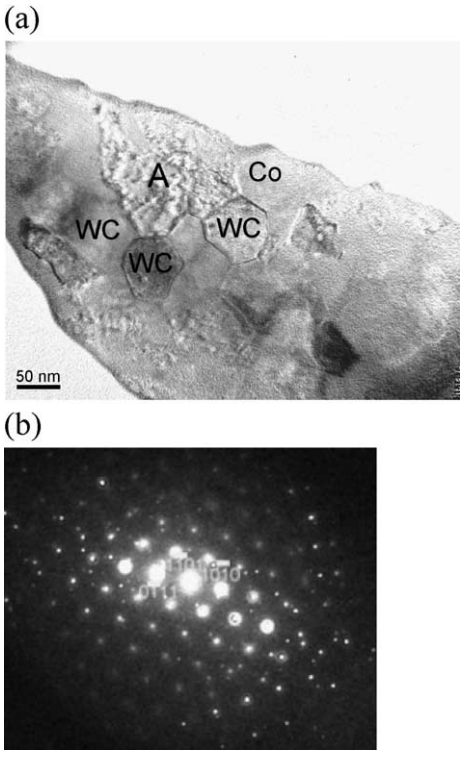

Fig. 5. Typical TEM microstructure of the SPS-treated WC–Co coating (a) showing that W_2C grains are surrounded by WC grains and Co; (b) shows a SAD pattern taken from the area A in (a), suggesting W_2C with hexagonal structure from the $(1\bar{2}1\bar{3})$ zone.

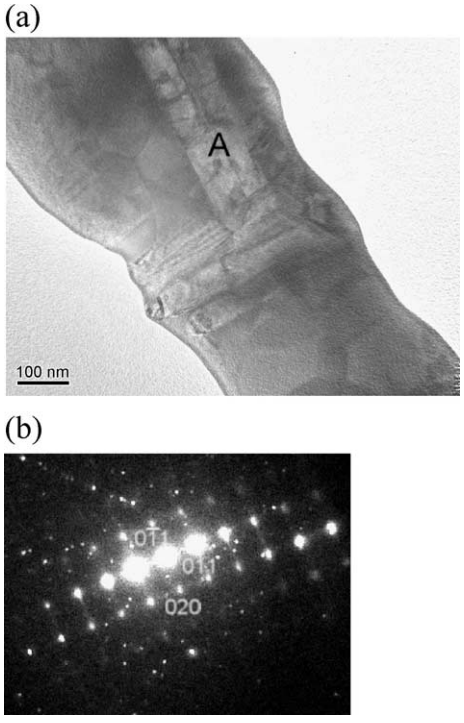

Fig. 6. Typical TEM microstructure of the SPS-treated WC–Co coating (a); (b) shows a SAD pattern taken from the area A in (a), suggesting Co_3W_3C with cubic structure from the [100] zone.

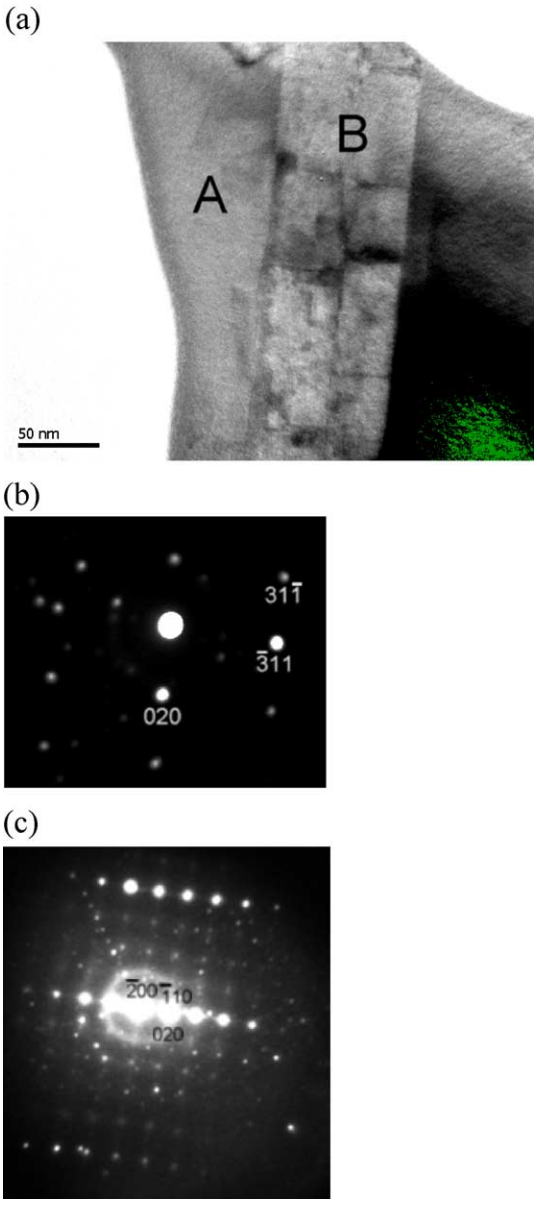

Fig. 7. Typical TEM microstructure of the SPS-treated WC–Co coating (a); (b) shows a SAD pattern taken from the area A in (a), suggesting Co with cubic structure from the [103] zone; and (c) shows a SAD pattern detected from the area B in (a), suggesting Co_3W_3C with cubic structure from the [001] zone.

WC particle, or the WC particle may reprecipitate and decarburize into W and C phases. Either one of these phenomena may result in recrystallization into the hard η phase, e.g., Co_3W_3C in the present case. The content of Co in the powders used in the present study is 12 wt.%. According to the diagram, it is reasonable that the formation of the η phase increased after the SPS treatment on the coatings. According to the W–C binary phase diagram (Fig. 9) [13], the increase in the carbon content effectively decreases the possibility of W_2C formation. During the SPS processing, due to the presence of micropores, local plasma discharges within the coating were generated. The

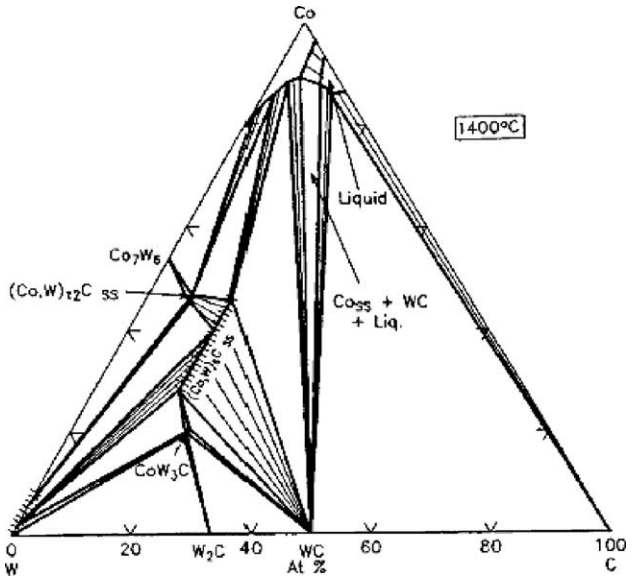

Fig. 8. The isothermal section of WC–Co phase diagram at 1425 °C (from Ref. [12]).

discharges could result in a local thermal spikes within the coating sample. The present SPS treatment on the plasma-sprayed WC–Co coatings confirmed the influence of the carbon content on the transformation of W_2C to WC. In addition, the WC–Co phase diagram also shows the influence of Co content on the phase changes during the high-temperature processing (plasma spraying and SPS treatment). The melting point of cobalt is 1495 °C. However, beyond 800 °C, WC and Co would form a solid solution, which favors the formation of Co_3W_3C. Such phase would improve the bonding among splats. This might be promising for the WC–Co coating since it was found that wear mainly occurred by the removal of splats or splat fragments [9]. In order to get further information about the effective thickness of the coatings with remarkable restoration of WC, X-ray photoelectron spectroscopy (XPS) profiling was conducted. The relative contents of C, Co, and W at different locations within the coatings were measured. It was found that carbon content decreases along the through-thickness direction from sample surface, which further indicates the limited carbon diffusion and effect of the extra carbon on the formation of WC. Only <10 μm coating was claimed to demonstrate the effective WC restoration.

During the rapid SPS processing, diffusion of carbon into the WC–Co coating and WC particles into Co binder would occur simultaneously. Therefore, the diffusivity of carbon plays a key role in determining the extent of the WC restoration. Previous study on the calculation of WC diffusion into Co during sintering of the powders showed that the diffusion equilibrium attained was influenced by sample geometry (e.g., thickness, etc.) and grain sizes [14]. A previous study has revealed the diffusion of WC particles into Co matrix and subsequent decarburization [10]. In that study, the nanosized WC grains in the as-sprayed coating (Fig. 3) might favor the diffusion during the SPS processing. Therefore, the intensified reaction between WC and Co brought about by the SPS treatment is a reasonable postulation. Based on the present result, a model can be proposed to illustrate the behavior of the WC–Co coatings during the SPS treatment: (1) diffusion of carbon into the coating through grain boundaries, (2) diffusion of WC into Co matrix, (3) WC restoration from W_2C and W, (4) formation of Co_3W_3C. It must be noted that these phenomena occurred simultaneously. A dense structure and improved splats' interface would be other outcome associating with the desirable phase changes. Much work needs to be conducted for a complete understanding of the WC restoration mechanism during the SPS treatment. In addition, the property enhancement of the WC–Co coatings by the SPS post-spray treatment has been clarified through microhardness evaluation. The microhardness (Vickers) of the coatings was measured from their polished cross-sections and surface as well using a HMV-2000 Shimadzu microhardness tester. For the coating surface, before the testing, the coatings were highly polished. A 300-g load was employed with a loading duration of 15 s. For each coating sample, a total of 20 readings were collected for an average value. It was found that the as-plasma-sprayed WC–Co coating showed a microhardness value (Hv_{300}) of 1010.9 (S.D.: 212.8) for its surface and 1080.1 (S.D.: 189.4) for its cross-section. Whilst the SPS-treated coating showed a microhardness value (Hv_{300}) of 1407.0 (S.D.: 205.9) for its surface and 1380.3 (S.D.: 194.5) for its cross-section at the WC restoration top layer, and 1175.5 (S.D.: 178.0) for its cross-section at other locations. It is clear that the SPS treatment caused a significant increase of microhardness, especially at the location where WC restoration was achieved. This, on the other hand, further proves the effective WC restoration at the top layer of the WC–Co coating through the SPS treatment.

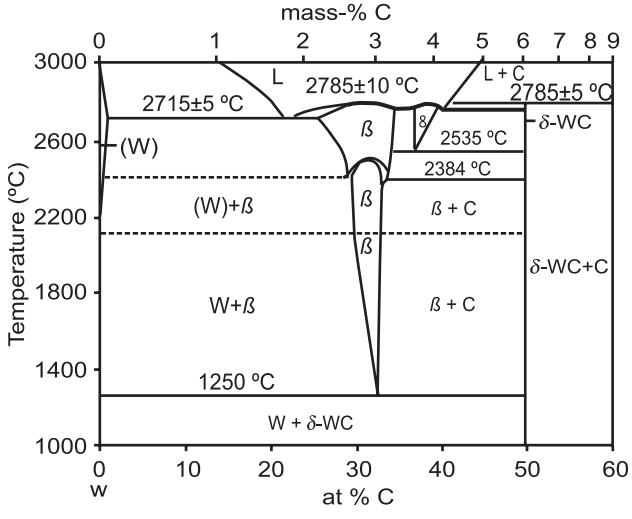

Fig. 9. W–C phase diagram at 1000–3000 °C, from Ref. [13].

4. Conclusions

The SPS post-spray processing at 800 °C and 6 min showed promising effect on the restoration of WC in the plasma-sprayed WC–Co coatings. Complete WC restoration at the coating surface was achieved successfully. Changes in microstructure, e.g., grain size growth, redistribution of different phases, was revealed within the coatings after SPS treatment. SPS-induced WC restoration can only be achieved within the coating surface with limited thickness (<10 μm), which depends on effective carbon diffusion. In the SPS-treated WC–Co coatings, an obvious layer of cubic Co_3W_3C ($\sim$ 80 nm) was revealed between Co and WC/W_2C. It indicates that SPS processing brought about further reaction between Co and WC/W_2C. Carbon diffusion, which is responsible for the WC restoration, and WC diffusion into Co, which accounts for forming Co_3W_3C phase, are the two main phenomena during the SPS processing the plasma-sprayed WC–Co coatings. Property enhancement was found through microhardness measurement whereby up to $\sim$ 40% improvement was recorded for the as-treated surface and polished cross-section of regions immediately underneath the surface. No significant improvement in microhardness value was detected in other parts of the SPS-treated coating.

References

[1] D.M. Kennedy, M. Helali, M.S.J. Hashmi, Surf. Coat. Technol. 68–69 (1994) 477.
[2] H. Liao, B. Normand, C. Coddet, Surf. Coat. Technol. 124 (2000) 235.
[3] R.S. Lima, J. Karthikeyan, C.M. Kay, J. Lindemann, C.C. Berndt, Thin Solid Films 416 (2002) 129.
[4] Y.C. Zhua, K. Yukimura, C.X. Ding, P.Y. Zhang, Thin Solid Films 388 (2001) 277.
[5] C. Verdon, A. Karimi, J.L. Martin, Mater. Sci. Eng., A 246 (1998) 11.
[6] B.H. Kear, G. Skandan, R.K. Sadangi, Scr. Mater. 44 (2001) 1703.
[7] D.A. Stewart, P.H. Shipway, D.G. McCartney, Surf. Coat. Technol. 105 (1998) 13.
[8] C.J. Li, G.C. Ji, Y.Y. Wang, K. Sonoya, Thin Solid Films 419 (2002) 137.
[9] Y. Qiao, T.E. Fischer, A. Dent, Surf. Coat. Technol. 172 (2003) 24.
[10] D.A. Stewart, P.H. Shipway, D.G. McCartney, Acta Mater. 48 (2000) 1593.
[11] L.G. Yu, K.A. Khor, H. Li, P. Cheang, Surf. Coat. Technol. 182 (2004) 308.
[12] A.E. McHale, Phase Equilibria Diagrams—Phase Diagrams for Ceramists, Vol. 10, The American Ceramic Society, Westerville, OH, 1994, p.893.
[13] T.B. Massalski (Ed.), Binary Alloy Phase Diagrams, Vol. 1: Alloys, Vol. 2: Phase Diagrams, ASM International, Materials Park, OH, 1990, p. 1116.
[14] S. Haglund, J. Ae Gren, Acta Mater. 46 (1998) 2801.